Published in final edited form as:
Proteins. 2010 September ; 78(12): 2638–2654. doi:10.1002/prot.22779.

The measured and calculated affinity of methyl and methoxy substituted benzoquinones for the Q_A site of bacterial reaction centers

Zhong Zheng[1], **P. Leslie Dutton**[2], and **M. R. Gunner**[1,*]

[1]Department of Physics, City College of New York, New York, NY 10031

[2]Department of Biochemistry and Biophysics, University of Pennsylvania, Philadelphia, PA 19104

Abstract

Quinones play important roles in mitochondrial and photosynthetic energy conversion acting as intramembrane, mobile electron and proton carriers between catalytic sites in various electron transfer proteins. They display different affinity, selectivity, functionality and exchange dynamics in different binding sites. The computational analysis of quinone binding sheds light on the requirements for quinone affinity and specificity. The affinities of ten oxidized, neutral benzoquinones (BQs) were measured for the high affinity Q_A site in the detergent solubilized *Rhodobacter sphaeroides* bacterial photosynthetic reaction center. Multi-Conformation Continuum Electrostatics (MCCE) was then used to calculate their relative binding free energies by Grand Canonical Monte Carlo sampling with a rigid protein backbone, flexible ligand and side chain positions and protonation states. Van der Waals and torsion energies, Poisson-Boltzmann continuum electrostatics and accessible surface area dependent ligand-solvent interactions are considered. An initial, single cycle of GROMACS backbone optimization improves the match with experiment as do coupled ligand and side chain motions. The calculations match experiment with an RMSD of 2.29 and a slope of 1.28. The affinities are dominated by favorable protein-ligand van der Waals rather than electrostatic interactions. Each quinone appears in a closely clustered set of positions. Methyl and methoxy groups move into the same positions as found for the native quinone. Difficulties putting methyls into methoxy sites are observed. Calculations using an SAS dependent implicit van der Waals interaction smoothed out small clashes, providing a better match to experiment with a RMSD of 0.77 and a slope of 0.97.

Keywords

quinone; bacterial reaction center; binding affinity; docking; Q_A; photosynthesis

Introduction

Quinones are the most important lipid-soluble electron and proton carriers in the membranes of mitochondria, chloroplasts and oxygenic bacteria.[1,2] They transfer electrons between proteins carrying out the proton-coupled electron transfer reactions that generate transmembrane proton gradients.[3,4] Quinone redox chemistry occurs in specific binding sites in these proteins, which favor binding different quinones[5] and modulate in situ quinone

*To whom correspondence should be addressed. Telephone: 212-650-5557. Fax: 212-650-6940. gunner@sci.ccny.cuny.edu.

Author Contributions: Z.Z. designed and guided the project and carried out all MCCE simulations; M.R.G. made the measurements of quinone affinity; P.L.D. advised on the selection of quinones and assay procedures; Z.Z. and M.R.G. wrote the paper. All authors discussed and edited the manuscript.

chemistry.[6-8] The biological quinone redox reactions shift the quinone between stable quinone and hydroquinone (quinol) species, requiring two electron and two proton transfers. The tuning of affinity, specificity and electrochemistry in protein is of prime importance since the intermediate, singly reduced semiquinone is a source of harmful reactive oxygen species (ROS).[9-12]

As quinones function as intermediaries in the bioenergetic transfer chain there are quinone binding sites in many proteins. The Krebs cycle products yield QH_2 via $NADH_2$ or succinate oxidation in NADH dehydrogenase (complex I) and succinate dehydrogenase (complex II).[13] In aerobic respiration, the cytochrome bc_1 complex gives electrons from QH_2 to cyt c,[8,14] which in turn reduces O_2 to water in cytochrome c oxidase. Different organisms can use different quinones. Animals and plants use only ubiquinone (UQ) in their mitochondrial membrane electron transfer proteins, while plants and algae use plastoquinone and phylloquinone in their chloroplast photosynthetic reactions. Bacteria use a mixture of quinones including UQ, menaquinone and rhodoquinone for photosynthetic and other transmembrane, bioenergetic reaction. Quinone binding sites are also the targets for anti-malarial drug,[15] antibiotics such as nafuredin,[16] and various herbicides.[17]

Quinones are seen in a slowly growing list of membrane protein crystal structures, including in photosynthetic reactions centers of bacteria (RCs) (Q_A, Q_B),[18] PSI and PSII,[19] cytochrome bc_1 and b_6f oxidoreductases (Q_o, Q_i),[20,21] quinol-fumarate reductase (Q_P,Q_D),[22] succinate dehydrogenase[12] and the enzyme DsbB.[23] However, inspection of these quinone binding sites does not provide a well-defined binding motif.[24] Binding sites have from 1 to 6 aromatic residues (Phe, Tyr and Trp) within 4Å of the quinone ring and tail. These can be parallel extensions of the quinone ring or lie over the ring in tilted or parallel orientations. The two quinone oxygens are hydrogen bond acceptors when the quinone is oxidized (Q) or donors in the neutral reduced cofactor (QH_2). Hydrogen bond partners found in the crystal structures include the ionizable Glu, Asp, Lys; the polar His, Ser, Tyr, and backbone NH. The number of hydrogen bond partners varies from 0 as for one of the two quinone binding sites in *Escherichia coli* fumarate reductase to 5 as in RCs. Water molecules are seen in about two thirds of the quinone binding sites.

The bacterial reaction centers of photosynthetic bacteria have proved to be a useful and robust system for experimental studies of quinone electrochemistry and binding.[25-27] The electrochemical midpoints, E_ms, of Q_A[6] and Q_B[28,29] of *Rb. sphaeroides* RC have been measured, even down to cryogenic temperature.[30,31] Computational analysis has followed. The Q to $Q^{\cdot-}$ E_m of the native UQ in the Q_A and Q_B sites have been satisfactorily calculated in wild type[32-36] and mutant RCs.[37] Likewise, the affinity of many compounds for the Q_A site of *Rb. sphaeroides* RCs have been measured, providing a qualitative picture of the importance of the quinone ring substituents and the tail structure.[5,38-44] However, there has been little computational analysis of quinone affinity. This is largely because calculations of binding affinity[45-48] are far more challenging than for E_ms and pK_as.[49-51]

The aim here is to measure and compute binding affinities to shed light on the native binding sites that are observed to accommodate quinones. The initial target is the primary quinone (Q_A) binding site of the photosynthetic reaction centers of *Rps. sphaeroides*. Methods to calculate ligand affinities need to combine search functions to generate ligand poses in the protein and scoring functions to rank their energies. All methods introduce simplifications in protein and ligand degrees of freedom and in the complexity of the scoring functions to increase the computational speed.[52-54] The fastest techniques use a rigid receptor and ligand, allowing only translation and rotation.[55] More refined methods such as DOCK,[56] AutoDock,[57] FlexE,[58] GOLD[59] provide the ligand with flexibility and the protein with limited flexibility. Inevitably conformational freedom greatly expands the size of the

problem. The relative protein-ligand interaction energies are evaluated with functions that range from simple statistical functions as found in QSAR,[60] to MM-PBSA or MM-GBSA[61,62] methods which use standard Molecular Dynamics (MD) bonded and non-bonded parameters and continuum electrostatics (CE) analysis[63] to more complete physics-based approaches with significant computational cost, such as alchemical free energy calculations[64] or DFT analysis.[65,66]

MCCE, a new MC-PBSA type method, which carries many novel features will be used here. It was initially developed for analysis of E_m and pK_a values and has been used extensively in the analysis of the quinone electrochemistry in RCs.[32,33,67,68] Recently MCCE has also been applied to analyze ion binding,[69] which represents an extension of the program to determine small molecule affinity. The binding of ten fully oxidized neutral benzoquinones (BQ) to the Q_A site of the *Rhodobacter sphaeroides* photosynthetic reaction center will be measured and then calculated. The considered interactions between the protein and the ligand combine molecular mechanics non-electrostatic interactions and Poisson-Boltzmann continuum electrostatics interactions. The binding affinity is determined with Grand Canonical Monte Carlo sampling (GCMC), which is ideal for studying binding as it allows the bound and free quinone to come to equilbrium.[70,71] MCCE allows flexible side chains[72] and multiple ligand binding poses[73] within a rigid backbone. Unlike almost all simulations, which need to pre-assign the ionization states of the protein and ligand, all protonation and redox states for each residue and cofactor can change in the Monte Carlo sampling that determines the ligand affinity. The importance of optimizing the backbone position, of the flexibility of the ligand position and the contribution of ligand rearrangement to the free energy of binding are evaluated. The results with a full AMBER van der Waals analysis of the quinone-protein non-electrostatic interactions is compared with an implicit, surface area dependent energy function.

Method

Measurement of quinone affinity

Rhodobacter sphaeroides bacteria, strain R-26, were grown anaerobically, photosynthetically, on succinate media. The RCs were extracted from the bacterial membrane with the detergent lauryldimethylamine oxide (LDAO), and purified by ammonium sulfate precipitation, followed by chromatography on a DEAE-cellulose column.[74] The bound primary and secondary quinones, Q_A, and Q_B, are removed from the protein by the method of Okamura[75] with minor modifications.[6] All Q_B is removed. The fraction residual Q_A is preparation dependent and varied from 0.01 to 0.15.

The source of the quinones can be found in ref [76]. The following abbreviations will be used henceforth: BQ: 1,4-benzoquinone; DQ: tetramethyl-BQ; Q_0: 2,3-dimethoxy-5-methyl-BQ and methyl-Q_0: 2,3-dimethoxy-5,6-methyl-BQ. Quinone purity was determined by HPLC chromatography, monitored at 220 and 250 nm.[77] Quinones were dissolved in ethanol or dimethylsulfoxide. Solutions of BQs with less than three substituents were made fresh immediately before use.

RC activity is monitored by the oxidation state of the bacteriochlorophyll dimer at 605 nm, as previously described.[78-80] If there is no active quinone present at the time of the flash the protein decays back to the ground state in 10 ns and no reaction is seen. Thus, this assay determines the K_d for quinone bound prior to the flash. If there is an active quinone correctly oriented, the state $P^+Q_A^-$ is formed, which lasts for milliseconds with the quinones tested here. The fraction of RCs with quinone bound is proportional to the ΔA_{605}.

The reaction mixture contains 0.10 to 0.35 μM Q_A-depleted RCs, solubilized by 2×10^{-4} to 10^{-3}% LDAO in 10 mM Tris-HCl at pH 8.0. The detergent in the assay mixture represents a dilution of that present in the RC stock solution. Measurements are initiated 30μs after a 10μs (full width at half maximum) xenon flash masked with an IR transmitting Kodak 88A wratten filter. Under these conditions ≈90% of the RC population absorbs at least one photon. The cuvette temperature is maintained at 22± l°C by a circulating water bath.

Calculation of quinone affinity

In MCCE analysis, the term ‘conformer’ specifies a specific position, protonation and redox state of a side chain or ligand. These are preselected during an initial sampling and optimization cycle (see reference [81] for a more complete description) and residues can have 1 to 100’s of conformers to choose from. The protein backbone is held fixed. Monte Carlo sampling then determines the Boltzmann distribution of conformers. Thus, all acidic and basic amino acids throughout the protein can be either protonated or deprotonated unless otherwise stated, while the side chains and ligands sample all, preselected positions. The conformer distribution is determined given the Poisson-Boltzmann electrostatic interactions and ligand solvation energies, full AMBER Lennard-Jones and torsion energies[82] and an SAS based non-electrostatic ligand-solvent interaction energy. The ligand affinity is derived from Grand Canonical Monte Carlo (GCMC) Sampling where the ligand can be bound to the protein or free in solution.[83] A similar GCMC analysis has been applied previously to calculate the chloride affinity to three proteins using MCCE.[69]

The generation of the pre-selected side chain conformers for final Monte Carlo sampling uses a multi-scale approach. This aspect of optimization of side chain and ligand positions is novel in MCCE and is described in detail below. MCCE QUICK conformer placing is the default for the protein as a whole.[81] This retains the input non-hydrogen (C,O,N,S) positions, while allowing additional, essentially isosteric positions for hydroxyls, His tautomers, and the interchange of the O and N in the Asn and Gln side chains. MCCE analysis then focuses more sampling of side chain positions near the quinone as described below. The program screens, optimizes and prunes these initial position conformers with an analytical energy function that includes AMBER torsion and Lennard-Jones energies as described in detail previously.[81] The electrostatic energies in the prescreening step are obtained using Coulomb’s law with a dielectric constant of 6. In the GCMC ligand binding analysis, DelPhi[84] is applied to solve the Poisson-Boltzmann equation with a protein dielectric of 4 and 80 for water at pH 7 and with 150 mM salt using Parse charges and radii. [85] AMBER[82] non-electrostatic parameters are applied for the Lennard-Jones and torsion energies. The quinone affinities are measured with solubilized protein, with the detergent kept below its critical micelle concentration so no membrane is included in the calculations.

During each Monte Carlo titration of ligand binding, the position of the four His (M266, M219, L190 and L230) and one Glu (M234) that are ligands to the RC iron atom are fixed in the crystal structure position and maintained with the His neutral, Glu ionized and Fe^{2+} state. This fixes the position and tautomer for His M219, which also makes a hydrogen bond to the quinone. All the bacteriochlorophylls, bacteriopheophytins and the ubiquinone at the Q_B site are fixed in their neutral ground state. There is an acidic cluster of Glu L212 and Asp L213 near the Q_B site. The acidic pair interacts strongly and the total net charge of the cluster remains -1.[33,36] Here Glu L212 is set to be neutral. In addition, Glu L104, which makes a hydrogen bond to the ring V keto carbonyl of bacteriopheophytin, is fixed in its protonated state. The ionization states of all other protonatable residues are determined by MCCE Monte Carlo sampling.

I. Preparation of protein structure file—Identical quinone docking and affinity calculations are carried out on 1AIJ[86] and 2UWU[87] structures taken from the Protein Data Bank (PDB).[88] They have a resolution of 2.20 and 2.04 Å respectively. All crystallographic water molecules, lipid and detergent molecules are removed.

Each of the ten BQs to be docked in the protein is optimized and its atomic electrostatic potential (ESP) partial charge distribution calculated using DFT analysis in the Gaussian98 program[89] with the UB3LYP/6-31G basis sets. This charge set was used in MCCE for the ligand within the protein and for reference calculations of the solvation energy in water.

One cycle of minimization is carried out for each ligand with the GROMACS molecular dynamics program.[90] These calculations use a reduced atomic model, where there are no hydrogens, so the quinone proton partial charge from the Gaussian98 analysis are redistributed to the closest carbon atom. The ab initio RC cofactor parameters derived by Ceccarelli, Procacci and Marchi[91] were converted to GROMACS format and used here. The bonded parameters for the other BQs needed for GROMACS were derived from the parameters for the native UQ.

II. Ligand Docking—The calculations start with the native quinone in the crystal structure stripped of substituents, leaving only the flat, six membered ring with the two para-carbonyl groups. MCCE adds the substituent methyl and methoxy groups to the ring, building the ten 1,4 BQs by applying information in topology files that define bond angles and length, and proton positions. Each BQ is docked in the protein in all possible poses taking into account the symmetry of the substituents. For example, while maintaining the positions of the two carbonyls, the methyl-1,4-BQ has four starting orientations with its methyl group docked into the four quadrants, while there is only one starting position needed for the 4-fold symmetrical DQ. This procedure initiates all subsequent calculations.

Each quinone undergoes one cycle of GROMACS optimization to relax the backbone (Figure 1,S1). GROMACS molecular dynamics can consider only one starting conformation for each residue and cofactor. As is unlikely that the cofactor can change substituent orientation during the short simulations used here, the most occupied MCCE quinone replacement orientation is added to the RC crystal structure as the GROMACS starting structure.[90] In addition, the side chain protonation states are fixed given the MCCE results. Ten cycles of energy minimization, each consisting of 500 0.002 ps steps are carried out on the whole protein for each quinone. Energy minimization uses the method of steepest descent. All runs converge in less than 500 steps. The RMSD for the changes in backbone generated by GROMACS in all structures is less than 0.11 Å for the whole protein and less than 0.14 Å in the region of the protein within15Å of the binding site. MCCE calculations with the different resultant protein backbone structures yield negligible differences in ionization state of the protein residues in the final calculations.

Multiple MCCE runs are used to generate many side chain rotamers and quinone positions for calculation of the relative affinity of each ligand. Each conformer generation cycle starts with the final GROMACS side chain and backbone positions for that ligand and the lowest energy ligand position found in the previous cycle of MCCE optimization (Figure 1). Side chain conformers are generated and optimized. Ligand conformers are constructed by a cycle of translation, out-of-plane rotation and then in-plane rotation. These are carried out independently to avoid an explosion of conformers (Figure S1). First ligand translation is carried out in 2 to 5 0.2~0.5 Å steps in each ±x,y,z directions. Four step translations create a 9^3 grid with ≈730 conformers. The final, lowest energy position is rotated out-of plane in 30° steps around three axes through the opposite carbons of the quinone ring plane (C1-C4, C3-C6 and C2-C5), yielding 12^3 conformers for each BQ orientation in the site. Finally, the

best position is subjected to in-plane rotation in 30° steps along each of the six axes perpendicular to the quinone plane through every ring carbon atom. Nearby side chain conformers are created and sampled with the quinone conformers in each cycle of optimization. Each type of ligand rotation is coupled to the swing function which allows each rotatable bond to move by 3.0°~ 5.0° for finer sampling. For each transformation stage 12 rotamers are created for each methoxy substituent's two rotatable bonds. In each cycle tens of thousands of conformers are made, screened with an analytical function leading to 10-30 positions that are subjected to Monte Carlo sampling with the complete energy function using Poisson-Boltzmann electrostatics and AMBER non-electrostatics parameters. All side chain and ligand conformers that are chosen to be bound to the protein in Monte Carlo sampling are saved and pooled.

The search for conformers is first conducted in an isolated 15Å protein sphere including the 160 residues around the quinone headgroup (Figure S1). For the ≈12 residues within 4Å of the quinone headgroup, 12 rotamers are made for each rotatable bond. QUICK rotamer making is used for the other residues.[81] For each quinone the ligand is translated and rotated as described above, side chain rotamers are made and their goodness assessed by MC sampling as described above. Then the same cycle of optimization is carried out in the full 840 residue protein. The calculation again starts with the protein residue positions taken from the GROMACS minimized structure. The ligand conformation is in a low energy position taken from the previous optimization cycle built in the 15Å sphere. The region where 12 side chain rotamers are considered for each bond is increased to ≈7Å from the quinone, now encompassing ≈35 residues. With the exception of the first pre-GROMACS calculations all occupied conformers from each stage of optimization are pooled and added to the subsequent cycles of Delphi calculation and Monte Carlo sampling. This builds up an extensive set of conformers to be included in the final Monte Carlo sampling that gives the quinone K_d. For each quinone the cycle of translation, in plane rotation, out of plane rotation and swing angular displacement is carried out 3 times in the 15Å sphere surrounding the quinone and then twice in the whole protein. The initial complete protein calculation starts with 10-30 thousand conformers. Analytical energy pre-screening functions reduce this to ≈2300 conformers, of which ≈450 are for the quinone and nearby residues. This increases to ≈2700 conformers after the first cycle and ≈3300 conformers following the second cycle of conformer optimization with ≈1500 conformers for the quinone and surroundings. Additional cycles of optimization are not found to increase the affinity showing the process has converged. Currently the entire procedure takes 3~5 days on a single 3.06 GHz processor.

III. Calculating the ligand binding energy—All protein and ligand conformers selected during the MCCE conformer generation cycles are preserved for the final analysis of the binding energy for that ligand. The bound ligand conformers compete against a conformer in solution, which has torsion, van der Waals self-energy and solvation energy of an isolated quinone in water and no interactions with the protein. The van der Waals and torsion energy for the solution conformer are taken from the most occupied conformer in the protein so that these non-electrostatic self-energy terms do not affect the affinity. The quinone titration is modeled by a series of Monte Carlo runs. An energy that is proportional to the effective chemical potential is added to the solution conformer to represent the effective concentration of the quinone.[69] When the calculated occupancy of the bound and free ligand is equal, the energy difference between the apo and holo states is zero. The quinone solution chemical potential that gives 50% bound ligand is compared for the various quinones to obtain the relative K_d.

The binding free energy is the change in the system free energy when a ligand in water binds to the RC Q_A site. Using the Boltzmann distribution of ligand and side chain conformers

found in the ligand titration, the binding energy can be decomposed in a mean field analysis as:[47]

$$\begin{aligned}\Delta G_{bind} &= \Delta G_{solv}+\Delta G_{P-L}+\Delta G_{entropy}+\Delta G_{strain}\\ &= (\Delta G_{solv,ele}+\Delta G_{solv,np})+(\Delta G_{prot,ele}+\Delta G_{prot,vdW})+\Delta G_{entropy}+\Delta G_{strain}\end{aligned} \quad (1)$$

ΔG_{solv} accounts for the loss of ligand-solvent interactions and $\Delta G_{P\text{-}L}$ the gain of new ligand-protein interactions. These terms may be favorable or unfavorable depending on the ligand, the solvent and the binding site. $\Delta G_{entropy}$ is a generally unfavorable term that accounts for the loss of degrees of freedom of the ligand on binding. ΔG_{strain}, accounts for the strain that builds up in the protein or ligand on binding.

ΔG_{solv}: The interaction of water and ligand is decomposed into three terms. The electrostatic component ($\Delta G_{solv,ele}$) accounts for the favorable interaction of water with the dipolar ligand. It is calculated by MCCE using DelPhi,[84] in which the solvent is modeled implicitly as a medium with a dielectric constant of 80 and the solute with an interior dielectric constant of 4. Experimentally it is expected that some water will occupy a site that is empty of quinone. No water enters the empty binding site and the dielectric constant remains 4 in the calculation. However, any errors that this yields should be the same for all quinones.

The non-polar solvation term consists of the unfavorable free energy required to form a cavity for the ligand in water (ΔG_{cav}), which is the basis of the hydrophobic effect[92] and the favorable solute-solvent van der Waals interaction (ΔG_{vdW}).[93,94] Both terms are estimated by an empirical linear relationship between the total non-polar solvation free energy ($\Delta G_{solv,np}$) and the solvent accessible area (A) so they cannot be readily separated. Here:

$$\begin{aligned}\Delta G_{solv} &= \Delta G_{solv,ele}+\Delta G_{solv,np}\\ &= \Delta G_{solv,ele}+(\gamma_1 A+B)=\Delta G_{solv,ele}+(\Delta G_{cav}+\Delta G_{vdW})\end{aligned} \quad (2)$$

where γ_1 is -5 cal·mol^{-1}·Å^{-2} and B is zero (Calc1 in Table 1).[95,96]

$\Delta G_{P\text{-}L}$: The protein-ligand contribution to the binding energy is also decomposed into electrostatic and non-electrostatic terms:

$$\Delta G_{P-L}=\Delta G_{prot,ele}+\Delta G_{prot,vdW} \quad (3)$$

Both contributions are treated explicitly in the full MCCE analysis. The electrostatic pair-wise interactions with the protein ($\Delta G_{prot,ele}$) are calculated by DelPhi.[84] The pair-wise van der Waals interactions ($\Delta G_{prot,vdW}$) are calculated using standard AMBER parameters.[82] Torsion energies are bundled into the latter term. Pair-wise terms are further decomposed into side chain and backbone interactions in the mean field analysis of the calculated quinone affinity.[81]

In addition, binding is analyzed using an implicit van der Waals protein-ligand interaction that is proportional to the ligand surface area (Calc2 in Table 1). Eqn 1 can be reorganized as:

$$\Delta G_{bind}=(\Delta G_{solv,np}+\Delta G_{prot,vdW})+(\Delta G_{solv,ele}+\Delta G_{prot,ele})+\Delta G_{entropy}+\Delta G_{strain} \quad (4a)$$

$$=\gamma_2 A+(\Delta G_{solv,ele}+\Delta G_{prot,elec})+\Delta G_{entropy}+\Delta G_{strain} \quad (4b)$$

The coefficient (γ_2) derived from the best fit line for the solvent accessible area (A) term is -55 cal·mol^{-1}·Å^{-2}.[97] This adds the favorable protein-ligand van der Waals interaction ($\Delta G_{prot,vdW}$) to the implicit water-ligand non-polar interactions (Eqn. 2). The electrostatic part of the binding energy ($\Delta G_{solv,ele}+\Delta G_{prot.ele}$), the change in entropic energy and the strain energy are the same in equations 4a and 4b.

$\Delta G_{entropy}$: Changes in entropy can make significant contributions to the overall free energy of ligand binding.[47,98,99] For extended ligands, simulations estimate that as much as 25 kcal/mol can be lost so the entropy loss can oppose binding nearly as strongly as the enthalpy favors it. However, the BQs considered here are flat six-member rings with at most two rotatable methoxy groups. The loss of rotational/translational entropy on being confined in the binding site is assumed to be the same for all ligands. Neglecting this term will contribute to the absolute calculated binding energies being more favorable than those measured. The configurational entropy loss is assumed to be proportional to the number of rotatable bonds affected by binding.[100-102] A range of values from 0.3,[103] 0.45,[104] to 0.7[105] kcal/mol per rotatable bond have been used in ligand binding simulations. Assuming the methoxy trans and ±gauche orientations yield three states of equal energy, when they are fixed in one location the entropy loss is:[105]

$$T\Delta S_{rot}=RT\ln 3 \approx 0.7 kcal/mol/methoxy \quad (5)$$

A correction of 0.7 kcal/mol/methoxy is used here for the 2,6-dimethoxy BQ. A smaller energy penalty of 0.4 kcal/mol/methoxy is used for the Q_0 and methyl-Q_0 because the adjacent methoxy groups restrict each other, so that one is in plane and the other out of plane even in solution.[5]

MCCE also makes an entropy correction when there are different numbers of conformers for distinguishable states.[81] Each quinone ligand has ≈20 different bound conformers competing with a single conformer representing the unbound state. The disparity in the number of conformers artificially favors the bound state. The entropy correction is calculated dynamically during Monte Carlo sampling to renormalize the number of low energy bound and free conformers.[81] The correction is generally less than 2 kcal/mol.

ΔG_{strain}: Upon binding, the protein and/or ligand may be distorted.[47] This costs energy, favoring the ligand in water. The strain energy is included in MCCE calculation when different conformations for the protein and ligand are adopted in the bound and unbound states. Thus, the Grand Canonical Monte Carlo sampling naturally includes this contribution to the free energy change.

Results & Discussion

The affinity of ten neutral benzoquinones (BQ) for the Q_A site of the *Rhodobacter sphaeroides* photosynthetic reaction center was measured with protein solubilized in detergent suspension below the critical micelle concentration. The relative binding free energies were then calculated using MCCE. The native quinone found in the crystal structure is Ubiquinone-10 (UQ_{10}), a 2,3-dimethoxy-5-methyl-6-isoprenyl-BQ with a 10 unit, 50 carbon, isoprene tail. Methyl-Q_0, a UQ analogue with a methyl group in place of the

isoprene tail, is chosen as the reference compound. Its K_d is measured to be 0.63 μM. All the values discussed below are relative to this quinone unless noted.

MCCE was developed to allow extensive rotamer sampling during calculations of residue and ligand pK_as and E_ms in proteins.[81] It has thus focused on processes that change the charge of the protein so electrostatic interactions are dominant. However, as side chain motions accompany protonation or redox changes, state energies also include Lennard-Jones and torsion terms. More recent calculations have used the Monte Carlo sampling of multiple positions and charge states to study proton coupled chloride binding.[69] In the work reported here the calculations of the affinities of quinones represent an extension of the program into the analysis of a redox active ligand. These binding free energy calculations compare affinities determined using implicit and explicit Lennard-Jones intra-protein interactions in two independent RC crystal structures. The computed results are in good agreement with the experimental affinity measurements, permitting an evaluation of the factors that generate the different affinities of the different compounds.

Experimental vs. Calculated relative binding free energies

Measured affinities—The measured affinities of the quinones for the Q_A binding site span 5.04 kcal/mol, from -0.14 kcal/mol for DQ to 4.90 kcal/mol for the unsubstituted BQ (Table 1). The standard deviation of the measurements is ≈0.25 kcal/mol. The overall trend is that the smaller quinones bind more weakly than the larger ones. The first methyl adds 0.3 kcal/mol to the affinity. Comparing the affinity of 2,3 dimethyl-BQ with the 2,5 and 2,6 isomers shows the second methyl adds ≈1.0 kcal/mol irrespective of its position. The third and fourth methyl raise the affinity by an additional ≈2 kcal/mol and ≈1.6 kcal/mol. Thus, the experimental results suggest that the first substituent to BQ adds less to the affinity than do the latter ones. Changing 2,6 dimethyl to 2,6-dimethoxy increases the affinity by 0.9 kcal/mol, while the methyl-Q_0 essentially binds as tightly as DQ.

Calculated affinities—The analysis presented here focuses on the relative rather than the absolute affinity of the BQs. The binding free energy calculations were compared in two crystal structures, 1AIJ and 2UWU (Table 1, Figure S2).[86,87] On average the binding energies relative to Methyl-Q_0, are 1.1 kcal/mol less favorable in 1AIJ than in 2UWU. This value is taken from the best-fit line in Figure S2. In 1AIJ the average error of the relative affinity is 0.72 kcal/mol, while it is -0.6 kcal/mol in 2UWU. With either structure the standard deviation of the error is 2.3 kcal/mol. The slope of the best-fit comparison between experiment and calculations is 1.28 for 1AIJ and 0.92 for 2UWU (Table 2). The results in the two crystal structures are highly correlated, with a slope of 1.0, R^2 of 0.83, and with no individual K_d differences >±2.5 kcal/mol (See Figure S2). Values in the text will refer to 1AIJ unless noted and will focus on the explicit van der Waals simulation (Calc1 in Table 1), since it provides the most structural information. The calculations are reasonably successful in reproducing the experimental values (Figure 2, Table 1). Seven out of nine calculated relative binding energies have errors with absolute value ≤ 2.0 kcal/mol. All side chain and ligand conformations selected by Monte Carlo sampling during multiple cycles of conformer generation are included in the final affinity calculation. The binding energy is found to increase relatively smoothly as additional conformers are added. However, when cycles of conformer additions beyond those described in the Methods sections were tested the calculated affinity varies by less than 0.4 kcal/mol, showing the process has converged (Supplementary Table 1).

Relaxation of the quinone in the binding site

The importance of protein flexibility in modulating site recognition in protein-ligand binding is well established.[53,106] However, a full analysis of all possible ligand protein

conformations is computationally very expensive. Additional degrees of freedom also introduce noise in the calculations due to fluctuations in the protein conformation that are unrelated to ligand binding. Here MCCE starts the calculation with ligand positions near the UQ_{10} bound in the structure rather than doing an exhaustive search for the best global ligand position. Following a single GROMACS relaxation of the protein, the protein backbone is fixed, while the side chains and ligands can sample multiple positions. This is similar to programs such as GLIDE,[107] which allow the protein side chains and ligand to make small movements to relieve the van der Waals clashes.

The analysis of the quinone affinity starts with the generation of conformers for the ligand and the protein. The quinones are first bound with the substituent added to the crystal structure Q_A ring. The quinone has two carbonyl groups, hydrogen bonded to Ala M260 (position 1) and His M219 (position 4), methoxy groups at ring carbons 3 (pointed towards Ile M265) and 2 (near Thr M261), a methyl group at carbon 5 (towards Met M218) and the tail at carbon 6 (near Met M256) (Figure 3,5). These numbers will be associated with the 6 orientations in the protein throughout the discussion. Asymmetric substituents are allowed to sample all 4 orientations in the proteins keeping the carbonyls fixed, yielding from one (BQ and DQ) to four (methyl-BQ, tri-methyl-BQ and Q_0) starting positions. A QUICK MCCE calculation of the energies of the distinguishable substituent orientations give differences in affinity for the best and worst orientations in the original crystal structure ranging from 11 (2,6-dimethyl BQ) to 28 kcal/mol (either dimethoxy BQ)(Table S1).

The crystal structure, with the ligand substituent pose at the lowest energy in an initial MCCE run, is minimized with GROMACS to relax the backbone. The affinity of the various BQs in their GROMACS optimized structures, were determined with a QUICK run with the quinone position fixed. This QUICK run binding energy is in some ways similar to a MM-PBSA analysis of a single protein docked ligand conformation with pre-assigned ionization states. However, the MCCE calculation still allows isosteric conformer positions and acidic and basic residue protonation states to be optimized in the calculation that determines the affinity.[81] A number of the smaller quinones show less than 1 kcal/mol difference in their affinity compared with that found for this quinone orientation in the original crystal structure. However, the backbone relaxation increases the affinity of DQ and 2,6-dimethoxy-BQ by ≈6 kcal/mol (Table S1). For Q_0 and methyl-Q_0 the single pose recovered from the GROMACS minimized structure binds 3~4 kcal/mol more weakly than the best quinone pose in the crystal structure. In both cases, the backbone van der Waals interactions are ≈5 kcal/mol more favorable in the minimized structure. However the 3-methoxy group, which is fixed in the QUICK run clashes with Thr M222 raising the energy by ≈7.5 kcal/mol. This will be relaxed when MCCE side chain optimization is added. The RMSD between experiment and the MCCE QUICK calculation following GROMACS backbone relaxation is 4.2 kcal/mol and the slope and R^2 are close to zero (Table 2).

DQ is the tightest binding quinone studied here with an affinity similar to methyl-Q_0, the analogue of the native UQ. However, it has the smallest affinity, 13 kcal/mol weaker than methyl-Q_0, when the methyl substituents are simply built onto the quinone ring in the crystal structure (Table S1). The MCCE QUICK run shows GROMACS optimization increases the DQ affinity by ≈6.7 kcal/mol by improving the van der Waals interactions, with negligible changes in the electrostatic energy. This is mostly due to changes in position of the Ala M249 and M260, which increases the affinity by ≈7.3 kcal/mol. The interaction of the DQ with the backbone of these two residues becomes ≈7.9 kcal/mol more favorable, while there are small unfavorable interactions with the side chain groups. The C_α hydrogen of M249 starts 1.6 Å from the DQ 2-methyl resulting in a 15.4 kcal/mol van der Waals clash (Figure 4). GROMACS relaxation increases this distance to 1.9 Å, reducing the energy to 4.8 kcal/mol. However, this pulls M260 closer, increasing the unfavorable interaction from 1.7 kcal/

mol to 4.4 kcal/mol. These compromises represent an example of the strain energy built up on binding. The RMSD changes for the two Ala backbones are each ≈0.45 Å. The significant GROMACS relaxation of 2,6-dimethoxy BQ results from the release of a similar clash between a methoxy and the backbone of Ala M260 (Figure 4).

Each GROMACS structure, optimized for each quinone, is now subjected to MCCE sampling of the side chain and ligand positions. This further increases the binding affinity by 0.3 to 7 kcal/mol. BQ, with the smallest van der Waals interactions, has the smallest and DQ the largest change. Small movements of DQ away from the GROMACS position considered above relieve clashes with the Ala M249 and Ala M260 backbone by ≈6 kcal/mol each. However the van der Waals interactions with the protein side chains, in particular Ile M265, become ≈4 kcal/mol less favorable. In total, the MCCE ensemble of accepted ligand and side chain position increases the DQ binding affinity by ≈7 kcal/mol. Thus, for the group of BQs coupled ligand, side chain and backbone relaxation is needed. While no dramatic conformational changes are found, small changes in the positions of the side chains of Ile M265, Met M262, Met M218, Thr M222 and Ile M223 lead to notable increase in the binding affinity.

Energy decomposition in the calculation of the quinone affinity

MCCE considers both explicit interactions, which depend on the atomic positions of the protein and ligand, and implicit energy terms, which depend on the atomic solvent-accessible surface area (SAS) or on the dielectric constant assigned to the protein and solvent. The implicit desolvation energy, and explicit electrostatic pair-wise interactions between the ligand and protein are obtained using DelPhi[84] to solve the Poisson Boltzmann equation. Explicit non-electrostatic Lennard-Jones and torsion energies are calculated with the AMBER force field.[82] An implicit non-polar solvation energy term combines the hydrophobic energy, favoring quinone binding and favorable Lennard-Jones interaction between the quinone and the solvent. A value of -5 cal·mol^{-1}·Å^{-2}, used here, is taken from an earlier analysis of the vacuum to water transfer free energy of 67 molecules, including analogs to the polar amino acid side chains and protein amide backbone, using Delphi electrostatic energy with PARSE charges as does MCCE.[95,96]

Electrostatic energies—The BQs whose affinities are calculated here are all neutral. As each has two carbonyls they are quadrapoles. The absolute total electrostatic contributions to binding range from -0.59 to -1.85 kcal/mol (Table 1). The biggest contributors are the ferrous non-heme iron that lies between Q_A and Q_B and His M219, which individually stabilize binding by up to 2.1 kcal/mol. The neutral His is both a ligand to the iron and a hydrogen bond donor to the quinone O_4. No other individual residue or backbone dipole has electrostatic interactions of more than 0.7 kcal/mol with any BQ. The loss in solvation energy, which opposes binding, is also not large, contributing from 1.5 to 2.7 kcal/mol. While the electrostatic interactions contribute a small amount to the affinity, they add 1.3 kcal/mol to the range of relative affinities of the different quinones. (See Table 1A) If the electrostatic interactions were ignored the average absolute error would increase from 1.75 to 2.0 kcal/mol.

One unique feature of the MCCE program is to be able to couple protein ionization with ligand binding. However, the quinone ligands studied here are neutral and situated at a relatively hydrophobic binding site. Thus calculated ionization states of the residues change little upon binding.

Non-electrostatic energies—The protein-ligand van der Waals interactions and the non-polar part of the solvation energy are the most significant contributors to the binding

affinity, both in magnitude and in their differences between different quinones (Table 1). These strongly distance sensitive interactions are the most dependent on the optimization of the quinone position in the binding site. After relaxation the favorable van der Waals interactions range from -20.86 (BQ) to -32.56 kcal/mol (2,6 dimethoxy BQ).

As the size of the ligand increases, these interactions generally become more favorable. The most important contributions are from Trp M252 and Ile M265, ≈3.5 Å away from the Q_A ring plane in the original crystal structure. The interactions with the Trp M252 side chain range from -2.0 (BQ) to -5.3 kcal/mol (methyl-Q_0). Mutation of this conserved Trp leads to an RC that will not bind Q_A.[108,109] The interactions with Ile M265 can be as favorable as -3 kcal/mol. Thr M222 and His M219 can also contribute ≈-2 kcal/mol each.

Two energies are summed in the implicit non-polar interaction of the ligand with the solvent. One is the unfavorable energy to create a cavity for the ligand in solution, which is the source of the hydrophobic effect.[110] The second is the favorable van der Waals interaction between the solvent and the ligand. Each of these is treated as being proportional to the surface area of the ligand (Eqn 2).[93] A value of -5 cal·mol^{-1}·Å^{-2} is used,[95,96] which favors moving the ligand out of the water. This provides a small contribution to the affinity ranging from 0.67 for unsubstituted BQ to 0.07 kcal/mol for Q_0 relative to methyl-Q_0 (Table 1).

BQ orientation in the Q_A site

Ligand conformers—MCCE generates multiple conformations for the ligands at the RC Q_A site. In the final analysis of affinity, there are usually ≈20 conformers available for each ligand. Monte Carlo sampling assigns occupancy for each one, ranking the quinone orientations in the binding site. All ten BQs have several closely clustered conformers occupied in the Boltzmann distribution of states (Figure 6). The optimized orientations provide a view of the local interactions around the quinone. When the original crystal structure with the substituted BQs in place of the native quinone is compared with the optimized protein structure with all selected ligand conformers, no large conformational changes are found. The binding site is quite flat, restricting rotation around the carbonyl axis so only positions in the native quinone plane are found (Figure 5B). The smallest quinone studied is the unsubstituted BQ, which is 4.9 Å wide including hydrogens, while 2,6 dimethoxy is the widest stretching ≈9 Å. The smaller BQ and methyl-BQ occupy a number of positions near the native quinone. As the quinone gets larger its position is better defined. Comparing only the six carbons in the quinone ring and two carbonyl oxygens, the RMSD between the crystal structure Q_A ring and the most favorable conformer of each ligand ranges from 0.17 Å in Q_0 to 2.6 Å in unsubstituted BQ. This clustering of the quinone in the binding site is not unexpected given that all of these BQs can reconstitute UQ function, which requires them to be in position to be reduced within 10 ns of the excitation of the reaction center.[79,80]

H-bonds to the ligand—The calculations can analyze the importance of specific interactions between the ligand and binding site. The two quinone carbonyls are hydrogen bond acceptors, O_4 from HN_δ of His M219 and O_1 from the backbone HN of Ala M260. However, a number of experiments have shown that the para-carbonyl arrangement is not required for binding or function.[42,79,111] A single carbonyl is sufficient for quinone binding.[42] The ortho-napthoquinone reconstitutes Q_A activity[112] and ortho-phenanthroline is an often-used competitive inhibitor for quinone binding.[113] Nevertheless, calculations here generally yield selected conformers with the two carbonyls pointing towards the native hydrogen partners (Figure 6).

The unsubstituted BQ was used to study the importance of the two H-bonds by rotating the ring moving the carbonyls from 1,4 to 2, 5 or 3, 6 orientations in the binding site (see Fig 5a). With the carbonyls in the 2,5 positions, overlaying a methyl and a methoxy in the native quinone, the quinone binds as tightly as in the 1,4 orientation. While the two H-bonds are lost weakening its electrostatic interactions with the protein by 2 and 1.2 kcal/mol respectively, there is now ≈3 kcal/mol more favorable van der Waals interactions with the protein. The affinity in the 3,6 orientation is 2 kcal/mol less. Thus for the unsubstituted neutral BQ, the carbonyl H-bonds are not indispensable for binding, though the rearrangement could change the reactivity.

The preferred methyl group positions—The first methyl increases the measured affinity by only 0.3 kcal/mol while the third increases it by 2.1 kcal/mol (Table 1). One challenge of the calculations is to explain these preferences. Methyl-1,4-BQ was built with its methyl group docked in each of the four quadrants (2, 3, 5 and 6) onto the UQ ring in the crystal structure. The relative affinity of each of the 4 orientations was determined by four separate binding calculations with only one conformer available in a QUICK MCCE calculation. The BQ with the methyl group in position 5 or 6 show very similar binding affinities (Figure 3). Adding a methyl group at position 3 is 4 kcal/mol less favorable. However the methyl is strongly disfavored at position 2, towards ThrM261, due to a clash between the methyl hydrogen and the C_α hydrogen of Ala M249 backbone. In the crystal structure there is a methoxy group at this position and the ether oxygen fits where the methyl does not. Thus the methyl, di-methyl and tri-methyl BQs place the first methyl group at position 5 or 6, with position 5 favored. Position 2 is filled only with DQ and requires backbone rearrangement and ligand movement. While this analysis was carried out with limited conformer sampling the same orientation preferences are found when the protein and ligand are allowed multi-conformer sampling. The calculated results do not fully explain the trend in binding affinity when adding methyl groups to the quinone ring. However it does show a strong preference for a methoxy rather than a methyl in this position, which contributes to the specificity of the binding site.

The distribution and orientation of the methoxy groups—There are three di-methoxy BQs studied here. In Q_0 and methyl-Q_0 the two methoxys are adjacent to each other. Monte Carlo sampling places these in protein positions 2, and 3, the same as the native quinone. This orientation binds ≈2 kcal/mol better than with the methoxys in protein positions 5 and 6 (Figure 3). The methoxy in the 2 position is required to reconstitute electron transfer from Q_A to Q_B in the RC.[5] The methoxy groups in the 2,6-dimethoxy-BQ each situated adjacent to the same carbonyl prefer protein positions 2 and 6 rather than 3 and 5 by ≈6 kcal/mol due to clashes with Ala M248 and Met M218. In addition, protein position 2 strongly prefers to bind a methoxy group rather than a methyl group sorting the methyl and methoxy groups into the same quadrants as found with the native UQ.

When a methoxy group lies in plane the oxygen lone pairs are conjugated with the π-orbital of the ring system. This increases the ring electron density, decreasing the quinone E_m and lowering the energy of the system, while an out of plane methoxy is electron withdrawing and at higher energy.[5] One consequence is that the methoxy position can tune the quinone redox potential, with an in plane substitution making the quinone harder to reduce.[5,114] For one methoxy group either with or without an adjacent methyl group, the in-plane conformation should be favored.[115] When there are two adjacent methoxy groups, steric hindrance only allows one to be in-plane at a time. Despite the potential importance of the methoxy position, recent investigation of 34 RC structures at better than 2.8Å resolution shows that the methoxy groups are not well anchored in the binding site by either a hydrogen bond to the ether oxygen or by strongly defined contacts.[116] The 3-methoxy group

was found at an angle of -77±8° while the 2-methoxy's position at 139±25° lies closer to being in plane, but is more variable.

Calculations were made with no special energy function applied to the methoxy positions. The standard van der Waals interactions will not allow two methoxys to both lie in plane, but did not account for the π electron donation into the ring that favors the in-plane orientation. The result is that all methoxy groups tend to lie out of plane with angles of 135.3±3.5°, 121±12.7° and 139.7±1° in the protein 3, 2 and 6 positions. Orientation 5 towards Met M218 is never occupied with a methoxy group.

Modification of the van der Waals terms

The van der Waals interactions, given by $A/r^{12} – B/r^{6}$, are exquisitely sensitive to the precise position of ligand and protein. Thus, small changes in orientation can change the ligand affinity by more than 20 kcal/mol (Table S1). The modest errors in the calculations with full MCCE treatment shows that this physics-based approach, developed for examining electrostatic interactions can also handle energies dominated by van der Waals interactions reasonably well. However, two alternative approaches that smooth these non-polar interactions were also investigated. In one the van der Waals energies were scaled, reducing the A and B coefficients by the same amount. In the second the non-polar energies were added solely with an implicit energy that is dependent on the surface area. The electrostatic desolvation energy and protein-ligand interactions continue to be taken from MCCE calculation based on the same multi-conformation protein structure and ligand positions.

The standard MCCE calculations use the full AMBER van der Waals potential. The slope for the comparison of experimental and calculated data is 1.28 implying MCCE overestimates the difference in interaction energy of the different compounds with the binding site (Table 2). The average explicit van der Waals energy is ≈ -81 $cal \cdot mol^{-1} \cdot Å^{-2}$. As described below an average van der Waals interaction of 50 $cal \cdot mol^{-1} \cdot Å^{-2}$ appears to provide a better estimate of the protein-ligand interactions, so both the A and B coefficients were reduced to 62% of their original values. The range of calculated binding affinities is now reduced from 10.7 kcal/mol to 6.7 kcal/mol, closer to the 5.0 kcal/mol found experimentally (Table 2). The RMSD is reduced from 2.29 to 1.4 and eight out of ten ligands have smaller errors.

A more extreme change is to treat the non-polar part of the protein-ligand interaction with another implicit, surface area dependent term, which is added to the non-polar solvation energy (Eqn 4). The best fit of the data and simulation comes with a surface area energy of -55 $cal \cdot mol^{-1} \cdot Å^{-2}$. Honig and coworkers have used a coefficient with a value of ≈-58 $cal \cdot mol^{-1} \cdot Å^{-2}$ for a similar analysis of the MHC class I protein-peptide binding.[97] Their calculated non-polar contribution to the binding free energy also favors ligand binding. The slope of the plot of experimental versus calculated relative binding free energy is now 0.97 with a R^2 of 0.84. As shown in Table 2 all measures of the correspondence between experimental and calculated affinities are improved (Figure 2, Table 2). The outliers remain the 2,6-dimethoxy BQ, with calculated value 1.4 kcal/mol more favorable and the unsubstituted BQ, which is 1.2 kcal/mol weaker than the measured value. While the analysis with the explicit van der Waals interactions shows that the MCCE sampling is able to generally find relatively good docked positions for each quinone, the excellent agreement with an implicit Lennard-Jones attraction shows that the Q_A binding site can easily accommodate the small quinones studied here.

The use of the fully implicit non-polar model mixes three surface dependent terms: the penalty for forming a cavity in water, the van der Waals interactions between solvent and solute and now the protein-ligand non-polar interactions. Here -5 $cal \cdot mol^{-1} \cdot Å^{-2}$ was used for

γ_1 to represent the non-polar solvation energy, a value that favors pushing the quinone into the protein (Eqn 2). Increasing this to -55 cal·mol^{-1}·Å^{-2} (γ_2) indicates an average of -50 cal·mol^{-1}·Å^{-2} for the protein-ligand van der Waals interactions. The water- cyclohexane partition coefficients (log P) have been measured for these ten BQs.[76,77] The best fit line for surface area dependence of the non-polar transfer free energy has a slope of ≈ -21 cal·mol^{-1}·Å^{-2}, which is the difference in the dispersion energy between water and hexane plus the unfavorable cavity term in water (Figure S3). This independently calculated value is smaller than the -55 cal·mol^{-1}·Å^{-2}, which is the best fit for the binding calculations using the implicit protein-ligand van der Waals energy. Thus, the average non-electrostatic protein-ligand interaction is approximately twice as favorable as the average interaction of the ligand with hexane.

Outliers in the calculations

The unsubstituted BQ, which binds too weakly and 2,6-dimethoxy, which binds too tightly are the two outliers in the calculations in both crystal structures. The analysis of the small, unsubstituted BQ turns out to be the most challenging. The affinity calculated with explicit Lennard Jones interactions is 2.2 (2UWU) to 4.8 (1AIJ) kcal/mol weaker than measured. It is the smallest BQ included here and is thus the most mobile in the binding site. More conformers are accepted with bigger movements than for any of the other BQ (Figure 6) so it may be we do not find the full range of favorable poses. Given its greater mobility in the site, the calculations may also overestimate the entropy loss. As the weakest binding quinone, it also contains more uncertainty in its measured affinity, as it can be difficult to achieve the necessary amounts of mono-disperse quinone in solution.

The 2,6-dimethoxy BQ binds especially tightly when compared with the 2,3-dimethoxy containing quinones with error from -3.7 (1AIJ) to -5.5 (2UWU) kcal/mol. One source of error can be not properly accounting for the cost of pushing the methoxy groups out of plane when they are bound. When the methoxy is forced to take conformations in the ring plane the affinity is weakened by ≈1 kcal/mol reducing the error.

Concluding Comments

Numerous different approaches have been used for calculating binding by docking and scoring,[54,117-119] each with their own strengths and limitations. Calculations can come to within 0.5 kcal/mol of the experimental values using time-intensive, advanced MD methods.[119] Faster methods using standard molecular-mechanics potential energy function can have a slope as steep as 1.77 with R^2 of 0.57 comparing experiment an calculation.[118] Recent explorations of different scoring functions in MM-GBSA yielded poor to modest results with R^2 values of 0.21-0.36.[117] All these indicate that protein-ligand binding remains a very challenging problem.

In this paper we describes a novel but computationally relatively inexpensive method to calculated binding affinities. MCCE combines pose generation and scoring. Flexibility is allowed for both ligand and protein side chains (but not backbone) using subroutines developed for exploration of side chain rotamer positions. The final calculation of affinity is carried out by Monte Carlo sampling of selected poses for ligand and side chains. Unlike almost all methods, which need to pre-assign the ionization states of the protein and ligand, all protonation and redox states for each residue and cofactor can also change in the Monte Carlo sampling that determines the ligand affinity. This unique feature allows study of the changes in the ionization states of the protein upon binding, which did not prove to be important here. However, it will permit analysis of the coupling of the changes in quinone electrochemistry to the differences in the binding affinity of the quinone and semiquinone.

With implicit protein ligand van der Waals interactions, the numerical results are improved, with a nearly ideal slope of 0.97 and a very good R^2 of 0.84. The success with implicit van der Waals interactions indicates that the solvent-accessible surface area correlates well with the protein-ligand van der Waals interactions as well as with the non-polar solvation energies. The Q_A binding site can generally accommodate these small compounds. The challenge then is to recover equally good results with a more complete model, which will provide more information about local interactions. A QUICK calculation of quinone binding affinity in the GROMACS optimized structure has an RMSD of 4.2 kcal/mol and an R^2 of ≈0 (Table 2). However, adding MCCE optimized conformers and calculating binding by Grand Canonical Monte Carlo sampling yield good results for the 10 quinones. The linear regression line comparing all measured and calculated K_ds has a slope of 1.28 with an R^2 of 0.54 using explicit van der Waals interactions. Thus, a single cycle of GROMACS backbone relaxation and full MCCE optimization of the ligand and side chain position is needed to relax small clashes that result within any rigid structure. The driving force for binding the neutral benzoquinone to the Q_A site is identified via calculation to be the protein-ligand van der Waals interaction, while the electrostatic energies contribute little. The favored distribution of the methyl and methoxy substitute on the benzoquinone ring is the same as the native quinone. In particular, quadrant 2 near ThrM261, binds a methoxy in the native UQ. A methyl will not bind in this position without changes in the backbone structure. Smaller quinones are more mobile at the binding site and allow more binding poses than larger quinones. In summary, calculations provide insight into how the Q_A binding site accommodates different type of quinones.

Supplementary Material

Refer to Web version on PubMed Central for supplementary material.

Acknowledgments

We thank Dr. Yifan Song for helpful discussion and for needed modifications of MCCE and Drs. Ceccarelli and Marchi for providing the parameters for bacterial reaction center cofactors in the GROMACS molecular dynamics simulations. We would like to acknowledge NSF MCB-0517589 (ZZ and MRG), GM 41048, GM27309 and DE-FG02-05ER46223 (PLD) and the infrastructure support of NIH 5G12 RR03060 at CCNY.

References

1. Nohl H, Kozlov AV, Staniek K, Gille L. The multiple functions of coenzyme Q. Bioinorganic Chem. 2001; 29:1–13.
2. Cramer, WA.; Knaff, DB. Energy Transduction in Biological Membranes: A Textbook of Bioenergetics. New York: Springer-Verlag; 1991.
3. Mitchell P. The protonmotive Q cycle: a general formulation. FEBS Lett. 1975; 59:137–139. [PubMed: 1227927]
4. Mitchell P. Protonmotive redox mechanism of the cytochrome bc_1 complex in the respiratory chain: protonmotive ubiquinone cycle. FEBS Lett. 1975; 56:1–6. [PubMed: 239860]
5. Wraight CA, Vakkasoglu AS, Poluektov Y, Mattis AJ, Nihan D, Lipshutz BH. The 2-methoxy group of ubiquinone is essential for function of the acceptor quinones in reaction centers from Rba. sphaeroides. Biochim Biophys Acta. 2008; 1777:631–636. [PubMed: 18474215]
6. Woodbury NW, Parson WW, Gunner MR, Prince RC, Dutton PL. Radical-pair energetics and decay mechanisms in reaction center containing anthraquinones or benzoquinones in place of ubiquinone. Biochim Biophys Acta. 1986; 851:6–22. [PubMed: 3524681]
7. Gunner MR, Madeo J, Zhu Z. Modification of quinone electrochemistry by the proteins in the biological electron transfer chains: examples from photosynthetic reaction centers. J Bioenerg Biomembr. 2008; 40:509–519. [PubMed: 18979192]

8. Rich PR. The quinone chemistry of bc complexes. Biochem Biophys Acta. 2004; 1658:165–171. [PubMed: 15282188]
9. Guo J, Lemire BD. The ubiquinone-binding site of the Saccharomyces cerevisiae succinate-ubiquinone oxidoreductase is a source of superoxide. J Biol Chem. 2003; 278:47629–47635. [PubMed: 13129931]
10. Borisov VB. Defects in mitochondrial respiratory complexes III and IV, and human pathologies. Mol Aspects Med. 2002; 23:385–412. [PubMed: 12231008]
11. Kramer DM, Roberts AG, Muller F, Cape J, Bowman MK. Q-cycle bypass reactions at the Q_o site of the cytochrome bc_1 (and related) complexes. Methods Enzymol. 2004; 382:21–45. [PubMed: 15047094]
12. Yankovskaya V, Horsefield R, Tornroth S, Luna-Chavez C, Miyoshi H, Leger C, Byrne B, Cecchini G, Iwata S. Architecture of succinate dehydrogenase and reactive oxygen species generation. Science. 2003; 299:700–704. [PubMed: 12560550]
13. Cecchini G, Maklashina E, Yankovskaya V, Iverson TM, Iwata S. Variation in proton donor/acceptor pathways in succinate:quinone oxidoreductases. FEBS Lett. 2003; 545:31–38. [PubMed: 12788489]
14. Hunte C, Palsdottir H, Trumpower BL. Protonmotive pathways and mechanisms in the cytochrome bc_1 complex. FEBS Lett. 2003; 545:39–46. [PubMed: 12788490]
15. Siregar JE, Syafruddin D, Matsuoka H, Kita K, Marzuki S. Mutation underlying resistance of Plasmodium berghei to atovaquone in the quinone binding domain 2 (Qo_2) of the cytochrome b gene. Parasitol Int. 2008; 57:229–232. [PubMed: 18248769]
16. Omura S, Miyadera H, Ui H, Shiomi K, Yamaguchi Y, Masuma R, Nagamitsu T, Takano D, Sunazuka T, Harder A, Kolbl H, Namikoshi M, Miyoshi H, Sakamoto K, Kita K. An anthelmintic compound, nafuredin, shows selective inhibition of complex I in helminth mitochondria. Proc Natl Acad Sci U S A. 2001; 98:60–62. [PubMed: 11120889]
17. Duke SO. Overview of herbicide mechanisms of action. Environ Health Perspect. 1990; 87:263–271. [PubMed: 1980104]
18. Stowell MHB, McPhillips TM, Rees DC, Soltis SM, Abresch E, Feher G. Light-induced structural changes in photosynthetic reaction center: implications for mechanism of electron-proton transfer. Science. 1997; 276:812–816. [PubMed: 9115209]
19. Heathcote P. Reaction centers: the structure and evolution of biological solar power. Trends Biochem Sci. 2002; 27:79–86. [PubMed: 11852245]
20. Gao X, Wen X, Esser L, Quinn B, Yu L, Yu CA, Xia D. Structural basis for the quinone reduction in the bc_1 complex: a comparative analysis of crystal structures of mitochondrial cytochrome bc_1 with bound substrate and inhibitors at the Q_i site. Biochemistry. 2003; 42:9067–9080. [PubMed: 12885240]
21. Kurisu G, Zhang H, Smith JL, Cramer WA. Structure of the cytochrome b_6f complex of oxygenic photosynthesis: tuning the cavity. Science. 2003; 302:1009–1014. [PubMed: 14526088]
22. Iverson TM, Arciero DM, Hooper AB, Rees DC. High-resolution structures of the oxidized and reduced states of cytochrome c_{554} from Nitrosomonas europaea. J Biol Inorg Chem. 2001; 6:390–397. [PubMed: 11372197]
23. Zhou Y, Cierpicki T, Jimenez RH, Lukasik SM, Ellena JF, Cafiso DS, Kadokura H, Beckwith J, Bushweller JH. NMR solution structure of the integral membrane enzyme DsbB: functional insights into DsbB-catalyzed disulfide bond formation. Mol Cell. 2008; 31:896–908. [PubMed: 18922471]
24. Fisher N, Rich PR. A motif for quinone binding sites in respiratory and photosynthetic systems. J Mol Biol. 2000; 296:1153–1162. [PubMed: 10686111]
25. Dutton, PL.; Gunner, MR.; Prince, RC. Trends in Photobiology. New York: Plenum Press; 1982. Systemmatic modification of electron transfer kinetics in a biological protein: Replacement of the primary ubiquinone of photochemical reaction centers with other quinones; p. 561-570.
26. Okamura MY, Paddock ML, Graige MS, Feher G. Proton and electron transfer in bacterial reaction centers. Biochim Biophys Acta. 2000; 1458:148–163. [PubMed: 10812030]

27. Wraight CA. Proton and electron transfer in the acceptor quinone complex of photosynthetic reaction centers from Rhodobacter sphaeroides. Front Biosci. 2004; 9:309–337. [PubMed: 14766369]
28. Mancino LJ, Dean DP, Blankenship RE. Kinetics and thermodynamics of the $P870^{+}Q_A^{-} \rightarrow P870^{+}Q_B^{-}$ reaction in isolated reaction centers from the photosynthetic bacterium *Rhodopseudomonas sphaeroides*. Biochim Biophys Acta. 1984; 764:46–54.
29. Kleinfeld D, Okamura MY, Feher G. Electron transfer in reaction centers of *Rhodopseudomonas sphaeroides*: I. Determination of the charge recombination pathway of $D^{+}Q_AQ_B^{-}$ and free energy and kinetic relations between $Q_A^{-}Q_B$ and $Q_AQ_B^{-}$ Biochim Biophys Acta. 1984; 766:126–140. [PubMed: 6331502]
30. Xu Q, Gunner MR. Temperature dependence of the free energy, enthalpy and entropy of $P^{+}Q_A^{-}$ charge recombination in photosynthetic reaction centers. J Phys Chem B. 2000; 104:8035–8043.
31. Xu Q, Gunner MR. Exploring the energy profile of the Q_A^{-} to Q_B electron transfer reaction in bacterial photosynthetic reaction centers: pH dependence of the conformational gating step. Biochemistry. 2002; 41:2694–2701. [PubMed: 11851416]
32. Alexov EG, Gunner MR. Calculated protein and proton motions coupled to electron transfer: electron transfer from Q_A^{-} to Q_B in bacterial photosynthetic reaction centers. Biochemistry. 1999; 38:8253–8270. [PubMed: 10387071]
33. Zhu Z, Gunner MR. Energetics of quinone-dependent electron and proton transfers in *Rhodobacter sphaeroides* photosynthetic reaction centers. Biochemistry. 2005; 44:82–96. [PubMed: 15628848]
34. Ishikita H, Knapp EW. Variation of Ser-L223 hydrogen bonding with the Q_B redox state in reaction centers from *Rhodobacter sphaeroides*. J Am Chem Soc. 2004; 126:8059–8064. [PubMed: 15212556]
35. Rabenstein B, Ullmann GM, Knapp EW. Electron transfer between the quinones in the photosynthetic reaction center and its coupling to conformational changes. Biochemistry. 2000; 39:10487–10496. [PubMed: 10956039]
36. Rabenstein B, Ullmann GM, Knapp EW. Energetics of electron-transfer and protonation reactions of the quinones in the photosynthetic reaction center of *Rhodopseudonas viridis*. Biochemistry. 1998; 37:2488–2495. [PubMed: 9485397]
37. Alexov E, Miksovska J, Baciou L, Schiffer M, Hanson DK, Sebban P, Gunner MR. Modeling the effects of mutations on the free energy of the first electron transfer from Q_A^{-} to Q_B in photosynthetic reaction centers. Biochemistry. 2000; 39:5940–5952. [PubMed: 10821665]
38. Stein RR, Castellvi AL, Bogacz JP, Wraight CA. Herbicide-quinone competition in the acceptor complex of photosynthetic reaction centers from *Rhodopseudomonas sphaeroides*: a bacterial model for PS-II-herbicide activity in plants. J Cell Biochem. 1984; 24:243–259. [PubMed: 6376526]
39. McComb JC, Stein RR, Wraight CA. Investigations on the influence of headgroup substitution and isoprene side-chain length in the function of primary and secondary quinones of bacterial reaction centers. Biochim Biophys Acta. 1990; 1015:156–171. [PubMed: 2404516]
40. Gunner, MR.; Braun, BS.; Bruce, JM.; Dutton, PL. Antennas and Reaction Centers of Photosynthetic Bacteria. Berlin: Springer-Verlag; 1986. The characterization of the Q_A binding site of the reaction center of *Rhodopseudomonas sphaeroides*; p. 298-305.
41. Warncke K, Gunner MR, Braun BS, Gu L, Yu C, Bruce JM, Dutton PL. Influence of hydrocarbon tail structure on quinone binding and electron-transfer performance at the Q_A and Q_B sites of the photosynthetic reaction center protein. Biochemistry. 1994; 33:7830–7841. [PubMed: 8011647]
42. Warncke K, Dutton PL. Experimental resolution of the free energies of aqueous solvation contributions to ligand-protein binding: quinone-Q_A site interactions in the photosynthetic reaction center protein. Proc Natl Acad Sci USA. 1993; 90:2920–2924. [PubMed: 8464908]
43. Takahashi E, Wells TA, Wraight CA. Protein control of the redox potential of the primary quinone acceptor in reaction centers from *Rhodobacter sphaeroides*. Biochemistry. 2001; 40:1020–1028. [PubMed: 11170424]
44. Hucke O, Schmid R, Labahn A. Exploring the primary electron aceptor (Q_A)-site of the bacterial reaction center from *Rhodobacter sphaeroides*: binding mode of vitamin K derivatives. Eur J Biochem. 2002; 269:1096–1108. [PubMed: 11856340]

45. Sousa SF, Fernandes PA, Ramos MJ. Protein-ligand docking: current status and future challenges. Proteins. 2006; 65:15–26. [PubMed: 16862531]
46. Jain AN. Scoring functions for protein-ligand docking. Curr Protein Pept Sci. 2006; 7:407–420. [PubMed: 17073693]
47. Gilson MK, Zhou HX. Calculation of protein-ligand binding affinities. Annu Rev Biophys Biomol Struct. 2007; 36:21–42. [PubMed: 17201676]
48. Brooijmans N, Kuntz ID. Molecular recognition and docking algorithms. Annu Rev Biophys Biomol Struct. 2003; 32:335–373. [PubMed: 12574069]
49. Garcia-Moreno EB, Fitch CA. Structural interpretation of pH and salt-dependent processes in proteins with computational methods. Methods Enzymology. 2004; 380:20–51.
50. Bashford D. Macroscopic electrostatic models for protonation states in proteins. Front Biosci. 2004; 9:1082–1099. [PubMed: 14977531]
51. Gunner MR, Mao J, Song Y, Kim J. Factors influencing energetics of electron and proton transfers in proteins. What can be learned from calculations. Biochim Biophys Acta. 2006; 1757:942–968. [PubMed: 16905113]
52. Kitchen DB, Decornez H, Furr JR, Bajorath J. Docking and scoring in virtual screening for drug discovery: methods and applications. Nat Rev Drug Discov. 2004; 3:935–949. [PubMed: 15520816]
53. Guvench O, MacKerell AD Jr. Computational evaluation of protein-small molecule binding. Curr Opin Struct Biol. 2009; 19:56–61. [PubMed: 19162472]
54. Singh N, Warshel A. Absolute binding free energy calculations: On the accuracy of computational scoring of protein-ligand interactions. Proteins. 2010; 78:1705–1723. [PubMed: 20186976]
55. Wiehe K, Peterson MW, Pierce B, Mintseris J, Weng Z. Protein-protein docking: overview and performance analysis. Methods Mol Biol. 2008; 413:283–314. [PubMed: 18075170]
56. Lang PT, Brozell SR, Mukherjee S, Pettersen EF, Meng EC, Thomas V, Rizzo RC, Case DA, James TL, Kuntz ID. DOCK 6: combining techniques to model RNA-small molecule complexes. RNA. 2009; 15:1219–1230. [PubMed: 19369428]
57. Morris GM, Huey R, Lindstrom W, Sanner MF, Belew RK, Goodsell DS, Olson AJ. AutoDock4 and AutoDockTools4: Automated docking with selective receptor flexibility. J Comput Chem. 2009; 30:2785–2791. [PubMed: 19399780]
58. Claussen H, Buning C, Rarey M, Lengauer T. FlexE: efficient molecular docking considering protein structure variations. J Mol Biol. 2001; 308:377–395. [PubMed: 11327774]
59. Verdonk ML, Cole JC, Hartshorn MJ, Murray CW, Taylor RD. Improved protein-ligand docking using GOLD. Proteins. 2003; 52:609–623. [PubMed: 12910460]
60. Gussio R, Pattabiraman N, Zaharevitz DW, Kellogg GE, Topol IA, Rice WG, Schaeffer CA, Erickson JW, Burt SK. All-atom models for the non-nucleoside binding site of HIV-1 reverse transcriptase complexed with inhibitors: A 3D QSAR approach. Journal of Medicinal Chemistry. 1996; 39:1645–1650. [PubMed: 8648604]
61. Stoica I, Sadiq SK, Coveney PV. Rapid and accurate prediction of binding free energies for saquinavir-bound HIV-1 proteases. J Am Chem Soc. 2008; 130:2639–2648. [PubMed: 18225901]
62. Rastelli G, Rio AD, Degliesposti G, Sgobba M. Fast and accurate predictions of binding free energies using MM-PBSA and MM-GBSA. J Comput Chem. 2009; 31:797–810. [PubMed: 19569205]
63. Zhang T, Koshland DE Jr. Computational method for relative binding energies of enzyme-substrate complexes. Protein Sci. 1996; 5:348–356. [PubMed: 8745413]
64. Mobley DL, Graves AP, Chodera JD, McReynolds AC, Shoichet BK, Dill KA. Predicting absolute ligand binding free energies to a simple model site. J Mol Biol. 2007; 371:1118–1134. [PubMed: 17599350]
65. Zhao Y, Truhlar DG. Infinite-basis calculations of binding energies for the hydrogen bonded and stacked tetramers of formic acid and formamide and their use for validation of hybrid DFT and ab initio methods. J Phys Chem A. 2005; 109:6624–6627. [PubMed: 16834013]
66. Sham YY, Chu ZT, Tao H, Warshel A. Examining methods for calculations of binding free energies: LRA, LIE, PDLD-LRA, and PDLD/S-LRA calculations of ligands binding to an HIV protease. Proteins: Struct Funct Genet. 2000; 39:393–407. [PubMed: 10813821]

67. Alexov EG, Gunner MR. Incorporating protein conformational flexibility into the calculation of pH-dependent protein properties. Biophys J. 1997; 72:2075–2093. [PubMed: 9129810]
68. Lancaster CRD, Michel H, Honig B, Gunner MR. Calculated coupling of electron and proton transfer in the photosynthetic reaction center of *Rhodopseudomonas viridis*. Biophys J. 1996; 70:2469–2492. [PubMed: 8744288]
69. Song Y, Gunner MR. Using multiconformation continuum electrostatics to compare chloride binding motifs in alpha-amylase, human serum albumin, and Omp32. J Mol Biol. 2009; 387:840–856. [PubMed: 19340943]
70. Clark M, Guarnieri F, Shkurko I, Wiseman J. Grand canonical Monte Carlo simulation of ligand-protein binding. J Chem Inf Model. 2006; 46:231–242. [PubMed: 16426059]
71. Clark M, Meshkat S, Wiseman JS. Grand canonical free-energy calculations of protein-ligand binding. J Chem Inf Model. 2009; 49:934–943. [PubMed: 19309088]
72. Zhao Y, Sanner MF. Protein-ligand docking with multiple flexible side chains. J Comput Aided Mol Des. 2008; 22:673–679. [PubMed: 18034309]
73. Guan Y, Shi R, Li X, Zhao M, Li Y. Multiple binding modes for dicationic Hoechst 33258 to DNA. J Phys Chem B. 2007; 111:7336–7344. [PubMed: 17530793]
74. Clayton RK, Wang RT. Photochemical reaction centers from Rhodopseudomonas spheroides. Methods Enzymol. 1971; 23:696–704.
75. Okamura MY, Isaacson RA, Feher G. The primary acceptor in bacterial photosynthesis: Obligatory role of ubiquinone in photoactive reaction centers of *Rhodopseudomonas sphaeroides*. Proc Natl Acad Sci USA. 1975; 72:3492–3496.
76. Keske, JM. Experimental and theoretical approaches to quinone binding and function at the Q_A site of photosynthetic reaction centers. Philadelphia: University of Pennslyvania;
77. Braun BS, Benbow U, Lloyd-Williams P, Bruce JM, Dutton PL. Determination of partition coefficients of quinones by high-performance liquid chromatography. Methods Enzymol. 1986; 125:119–129. [PubMed: 3713532]
78. Dutton PL, Petty KM, Bonner HS, Morse SD. Cytochrome C_2 and Reaction Center of Rhodospeudomonas-Spheroides Ga Membranes - Extinction Coefficients, Content, Half-Reduction Potentials, Kinetics and Electric-Field Alterations. Biochim Biophys Acta. 1975; 378:536–556. [PubMed: 237543]
79. Gunner MR, Robertson DE, Dutton PL. Kinetic studies on the reaction center protein from *Rhodopseudomonas sphaeroides*: The temperature and free energy dependence of electron transfer between various quinones in the Q_A site and the oxidized bacteriochlorophyll dimer. J Phys Chem. 1986; 90:3783–3795.
80. Gunner MR, Dutton PL. Temperature and -ΔG° dependence of the electron transfer from BPh^- to Q_A in reaction center protein from *Rhodobacter sphaeroides* with different quinones as Q_A. J Am Chem Soc. 1989; 111:3400–3412.
81. Song Y, Mao J, Gunner MR. MCCE2: improving protein pKa calculations with extensive side chain rotamer sampling. J Comput Chem. 2009; 30:2231–2247. [PubMed: 19274707]
82. Pearlman DA, Case DA, Caldwell JW, Ross WS, Cheatham TE III, DeBolt S, Ferguson D, Seibel G, Kollman P. AMBER a package of computer programs for applying molecular mechanics. normal mode analysis, molecular dynamics and free energy calculations to simulate the structural and energetic properties of molecules. Computer Physics Communications. 1995; 91:1–41.
83. Liwo A, Czaplewski C, Oldziej S, Scheraga HA. Computational techniques for efficient conformational sampling of proteins. Curr Opin Struct Biol. 2008; 18:134–139. [PubMed: 18215513]
84. Nicholls A, Honig B. A rapid finite difference algorithm utilizing successive over-relaxation to solve the Poisson-Boltzmann equation. J Comp Chem. 1991; 12:435–445.
85. Sitkoff D, BenTal N, Honig B. Calculation of alkane to water solvation free energies using continuum solvent models. J Phys Chem-Us. 1996; 100:2744–2752.
86. Stowell MH, McPhillips TM, Rees DC, Soltis SM, Abresch E, Feher G. Light-induced structural changes in photosynthetic reaction center: implications for mechanism of electron-proton transfer. Science. 1997; 276:812–816. [PubMed: 9115209]

87. Koepke J, Krammer EM, Klingen AR, Sebban P, Ullmann GM, Fritzsch G. pH modulates the quinone position in the photosynthetic reaction center from Rhodobacter sphaeroides in the neutral and charge separated states. J Mol Biol. 2007; 371:396–409. [PubMed: 17570397]

88. Berman HM, Westbrook J, Feng Z, Gilliland G, Bhat TN, Weissig H, Shindyalov IN, Bourne PE. The Protein Data Bank. Nucleic Acids Research. 2000; 28:235–242. [PubMed: 10592235]

89. Frisch, MJ.; Trucks, GW.; Schlegel, HB.; Scuseria, GE.; Robb, MA.; Cheeseman, JR.; Zakrzewski, VG.; Montgomery, JA., Jr; Stratmann, RE.; Burant, JC.; Dapprich, S.; Millam, JM.; Daniels, AD.; Kudin, KN.; Strain, MC.; Farkas, O.; Tomasi, J.; Barone, V.; Cossi, M.; Cammi, R.; Mennucci, B.; Pomelli, C.; Adamo, C.; Clifford, S.; Ochterski, J.; Petersson, GA.; Ayala, PY.; Cui, Q.; Morokuma, K.; Malick, DK.; Rabuck, AD.; Raghavachari, K.; Foresman, JB.; Cioslowski, J.; Ortiz, JV.; Baboul, AG.; Stefanov, BB.; Liu, G.; Liashenko, A.; Piskorz, P.; Komaromi, I.; Gomperts, R.; Martin, RL.; Fox, DJ.; Keith, T.; Al-Laham, MA.; Peng, CY.; Nanayakkara, A.; Challacombe, M.; Gill, PMW.; Johnson, B.; Chen, W.; Wong, MW.; Andres, JL.; Gonzalez, C.; Head-Gordon, M.; Replogle, ES.; Pople, JA. Gaussian 98, Revision A.9. Gaussian, Inc.; Pittsburgh PA: 1998.

90. Van Der Spoel D, Lindahl E, Hess B, Groenhof G, Mark AE, Berendsen HJ. GROMACS: fast, flexible, and free. J Comput Chem. 2005; 26:1701–1718. [PubMed: 16211538]

91. Ceccarelli M, Procacci P, Marchi M. An ab initio force field for the cofactors of bacterial photosynthesis. J Comput Chem. 2003; 24:129–142. [PubMed: 12497594]

92. Kauzmann W. Some factors in the interpretation of protein denaturation. Adv Protein Chem. 1959; 14:1–63. [PubMed: 14404936]

93. Levy RM, Zhang LY, Gallicchio E, Felts AK. On the nonpolar hydration free energy of proteins: surface area and continuum solvent models for the solute-solvent interaction energy. J Am Chem Soc. 2003; 125:9523–9530. [PubMed: 12889983]

94. Wagoner JA, Baker NA. Assessing implicit models for nonpolar mean solvation forces: the importance of dispersion and volume terms. Proc Natl Acad Sci U S A. 2006; 103:8331–8336. [PubMed: 16709675]

95. Ben-Naim A, Marcus Y. Solvation thermodynamics of nonionic solutes. J Chem Phys. 1984; 81:2016–2027.

96. Sitkoff D, Sharp KA, Honig B. Accurate calculation of hydration free energies using macroscopic solvent models. J Phys Chem. 1994; 98:1978–1988.

97. Froloff N, Windemuth A, Honig B. On the calculation of binding free energies using continuum methods: application to MHC class I protein-peptide interactions. Protein Science. 1997; 6:1293–1301. [PubMed: 9194189]

98. Chang CE, Chen W, Gilson MK. Ligand configurational entropy and protein binding. Proc Natl Acad Sci U S A. 2007; 104:1534–1539. [PubMed: 17242351]

99. Villa J, Strajbl M, Glennon TM, Sham YY, Chu ZT, Warshel A. How important are entropic contributions to enzyme catalysis? Proc Natl Acad Sci U S A. 2000; 97:11899–11904. [PubMed: 11050223]

100. Bohm HJ. The development of a simple empirical scoring function to estimate the binding constant for a protein-ligand complex of known three-dimensional structure. J Comput Aided Mol Des. 1994; 8:243–256. [PubMed: 7964925]

101. Eldridge MD, Murray CW, Auton TR, Paolini GV, Mee RP. Empirical scoring functions: I. The development of a fast empirical scoring function to estimate the binding affinity of ligands in receptor complexes. J Comput Aided Mol Des. 1997; 11:425–445. [PubMed: 9385547]

102. Wang R, Lai L, Wang S. Further development and validation of empirical scoring functions for structure-based binding affinity prediction. J Comput Aided Mol Des. 2002; 16:11–26. [PubMed: 12197663]

103. Luo R, Gilson MK. Synthetic adenine receptors: Direct calculation of binding affinities. J Amer Chem Soc. 2000; 122:2934–2937.

104. Nicholls A, Sharp K, Honig B. Protein folding and association: insights from the interfacial and thermodynamic properties of hydrocarbons. Proteins: Struct Funct Genet. 1991; 11:281–296. [PubMed: 1758883]

105. Ajay, Murcko MA. Computational methods to predict binding free energy in ligand-receptor complexes. J Med Chem. 1995; 38:4953–4967. [PubMed: 8544170]
106. Wong CF, McCammon JA. Protein flexibility and computer-aided drug design. Annu Rev Pharmacol Toxicol. 2003; 43:31–45. [PubMed: 12142469]
107. Zavodszky MI, Sanschagrin PC, Korde RS, Kuhn LA. Distilling the essential features of a protein surface for improving protein-ligand docking, scoring, and virtual screening. J Comput Aided Mol Des. 2002; 16:883–902. [PubMed: 12825621]
108. Stilz HU, Finkele U, Holzapfel W, Lauterwasser C, Zinth W, Oesterhelt D. Influence of M subunit Thr222 and Trp252 on quinone binding and electron transfer in Rhodobacter sphaeroides reaction centres. Eur J Biochem. 1994; 223:233–242. [PubMed: 8033896]
109. McAuley KE, Fyfe PK, Ridge JP, Cogdell RJ, Isaacs NW, Jones MR. Ubiquinone binding, ubiquinone exclusion, and detailed cofactor conformation in a mutant bacterial reaction center. Biochemistry. 2000; 39:15032–15043. [PubMed: 11106481]
110. Pratt LR, Chandler D. Theory of the hydrophobic effect. J Chem Phys. 1977; 67:3683–3705.
111. Morris AL, Synder SW, Zhang Y, Thurnauer MC, Dutton PL, Robertson DE, Gunner MR. Electron spin polarization model applied to sequential electron transfer in iron-containing photosynthetic bacterial reaction centers with different quinones as Q_A. J Phys Chem. 1995; 99:3854–3866.
112. Gunner MR, Nicholls A, Honig B. Electrostatic potentials in *Rhodopseudomonas viridis* reaction center: Implications for the driving force and directionality of electron transfer. J Phys Chem. 1996; 100:4277–4291.
113. Okamura MY, Isaacson RA, Feher G. Primary acceptor in bacterial photosynthesis: obligatory role of ubiquinone in photoactive reaction centers of Rhodopseudomonas spheroides. Proc Natl Acad Sci U S A. 1975; 72:3491–3495. [PubMed: 1081231]
114. Prince RC, Dutton PL, Bruce JM. Electrochemistry of ubiquinones, menaquinones and plastoquinones in aprotic solvents. FEBS Letts. 1983; 160:273–276.
115. Nonella M, Boullais C, Mioskowski C, Nabedryk E, Breton J. vibrational spectrum and torsional potential of 2-methoxy-3-methyl-1,4-benzoquinone. J Phys chem. 1999; 103:6363–6370.
116. Wraight, CA.; Gunner, MR. The Acceptor Quinones of Purple Photosynthetic Bacteria - Structure and Spectroscopy. Springer; Netherlands: 2008.
117. Yang CY, Sun H, Chen J, Nikolovska-Coleska Z, Wang S. Importance of ligand reorganization free energy in protein-ligand binding-affinity prediction. J Am Chem Soc. 2009; 131:13709–13721. [PubMed: 19736924]
118. Boas FE, Harbury PB. Design of protein-ligand binding based on the molecular-mechanics energy model. J Mol Biol. 2008; 380:415–424. [PubMed: 18514737]
119. Jiao D, Golubkov PA, Darden TA, Ren P. Calculation of protein-ligand binding free energy by using a polarizable potential. Proc Natl Acad Sci U S A. 2008; 105:6290–6295. [PubMed: 18427113]

Abbreviations

MCCE	Multi-conformation Continuum Electrostatics
MC	Monte Carlo
MM-PBSA	Molecular Mechanics-Poisson Boltzmann Surface Area method
MM-GBSA	Molecular Mechanics-Generalized Poisson Boltzmann Surface Area method
ESP	electrostatic potential charge
GCMC	Grand Canonical Monte Carlo
UQ	ubiquinone
BQ	benzoquinone

DQ	tetramethyl-BQ
Q_0	2,3-dimethoxy, 5-methyl-BQ
methyl-Q_0	2,3-dimethxy, 5,6-methyl-BQ
RC	reaction center

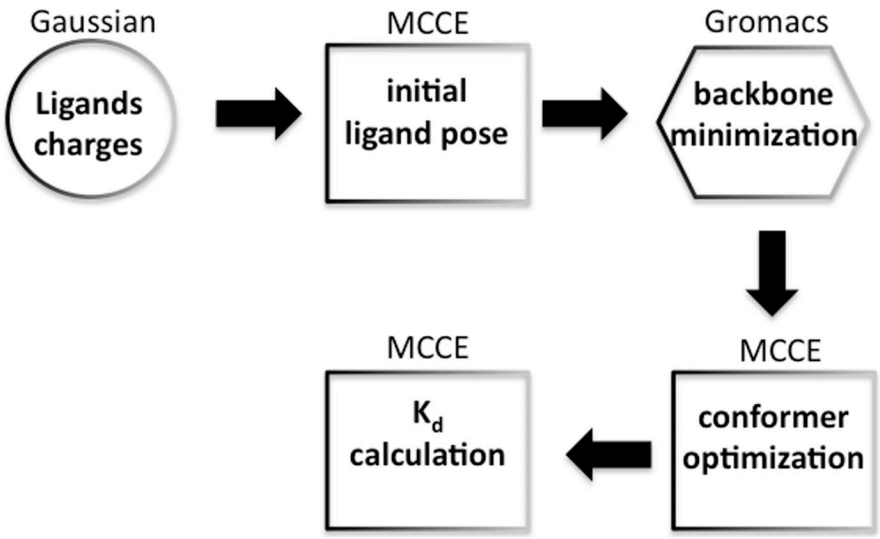

Figure 1.

Overview of K_d calculations. Gaussian generates ESP charges for quinone in a given redox and protonation state. MCCE finds lowest energy substituent orientation starting from native quinone ring. This conformer is added to GROMACS energy minimization of backbone and side chains. The GROMACS derived backbone will be used for all subsequent MCCE runs with this ligand. MCCE generates potential side chain and ligand conformers through cycles of translation, out-of-plane and then in-plane rotation. Good poses are further optimized with smaller motions. MCCE K_ds are obtained by competing bound and free ligands in Grand Canonical Monte Carlo sampling as a function of quinone concentration. This uses the full energy function and all protein and ligand conformers selected in any round of conformer optimization merged onto the same backbone.

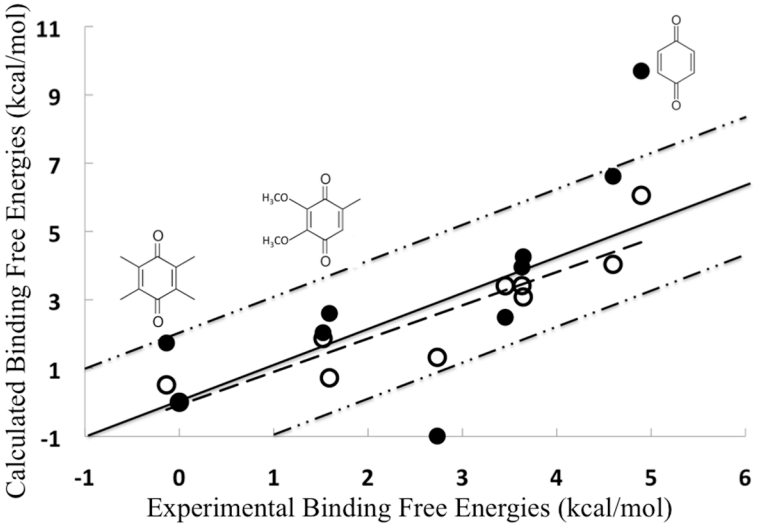

Figure 2.

Experimental vs. calculated binding free energies (kcal/mol). (●): Explicit AMBER Lennard- Jones energies. Dashed-dotted lines show errors of ±2 kcal/mol. Eight out of ten quinones are within this range. The best fit slope is 1.28 with a RMSD of 2.29. (○): Implicit SAS term for protein-ligand Lennard-Jones interactions. The average |error| is now 0.64±0.44 kcal/mol. Dashed line: best fit line with a slope of 0.97 and R^2 of 0.84.

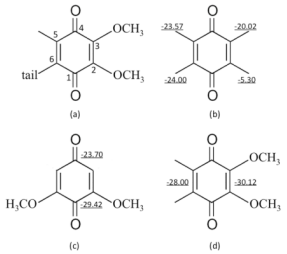

Figure 3.

(a) The headgroup of the native quinone. The carbons on the ring are labeled from 1 to 6. The native ubiquinone has two carbonyl groups, hydrogen bonded to Ala M260 (position 1) and His M219 (position 4), methoxy groups at ring carbons 2 (near Thr M261) and 3 (near Ile M265) and, a methyl group at carbon 5 (towards Met M218) and the tail at carbon 6 (near Met M256). These orientations are used throughout the paper. (b-d) The energy in kcal/mol of each orientation is in the protein is underlined. (b) Energies for methyl groups in methyl-BQ docked into the four quadrants onto the crystal structure ring. Position 6 is the most favorable. (c) The 2,6 di-methoxy BQ is docked with the Methoxyls in the 2,6 or the 3, 5 positions. The first is at lower energy. (d) The Methyl-Q_0 is docked with the methoxys in the 2,3 or the 5,6 positions. The former is favored.

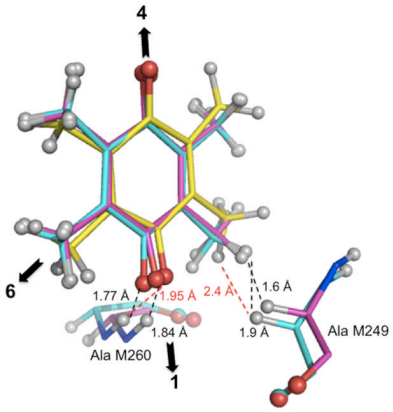

Figure 4.

The overlap of DQ and the backbone of Ala M249 and Ala M260 in crystal structure (magenta), GROMACS minimized structure (cyan) and MCCE optimized structure (yellow). The backbone amides are identical in GROMACS and MCCE structures so only the cyan is seen. Dashed lines label the distance between the quinone and the backbones of the two Ala residues. Black: crystal structure and GROMACS structure. Red: MCCE structure. The black arrows label the direction of the quadrants. Position 6 is occupied by the quinone tail in the native UQ_{10}.

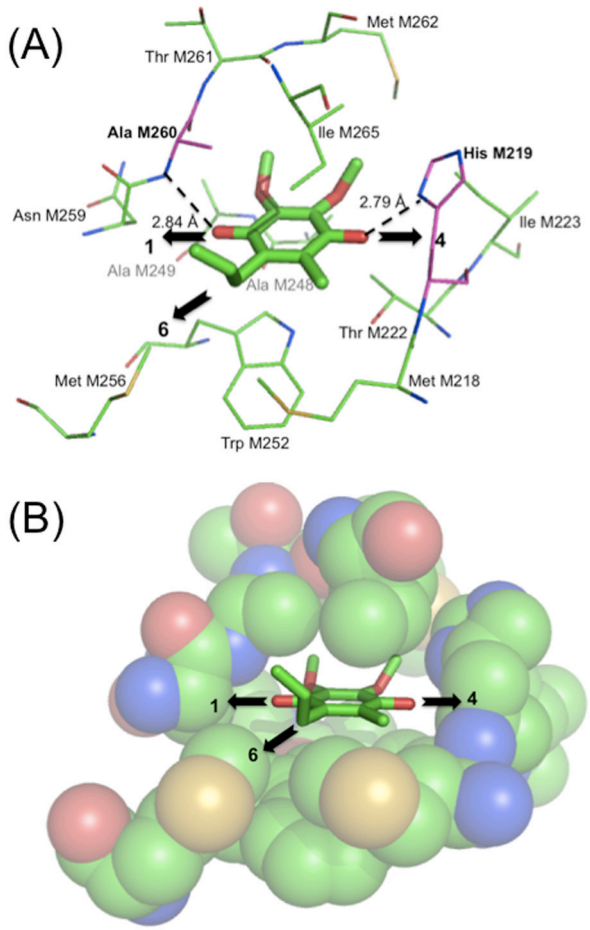

Figure 5.

Residues within 4Å of the Q_A headgroup. A and B are both views close to the ring plane but from slightly different angles. The same residues are shown in the two figures. The two H-bond partners to the ubiquinone are Ala M260 and His M219, which are highlighted in magenta in A. The black arrows label the quadrant designation. Figure B shows the binding site is too flat to allow significant rotation of the quinone out of plane.

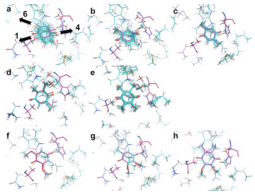

Figure 6.

The overlap of the crystal structure (magenta) with the final MCCE minimized structures with all selected protein and ligand conformers (blue). a: unsubstituted BQ, b: methyl-BQ, c: 2,5 di-methyl-BQ, d: tri-methyl-BQ, e: DQ, f: 2,6 di-methoxy BQ, g: Q_0, h: methyl-Q_0. The two H-bond partners to the ubiquinone, Ala M260 and His M219 and the most occupied ligand conformer are thicker sticks. As the ligand gets smaller more ligand poses are observed.

Table 1

A,B: Relative experimental and calculated binding energies using methyl-Q_0 as the reference compound. Results of multiple calculations vary by <0.4 kcal/mol, while the experimental results have errors of ≈0.25 kcal/mol. A: Calculation in crystal structure 1AIJ. B: 2UWU. C: absolute experimental and calculated binding energies in 1AIJ. Calc[1] with vdW[1] represents full MCCE binding calculations with AMBER protein-ligand van der Waals interactions and -5 cal/mol/Å^2 surface area dependent ligand-solvent non-electrostatic interactions (Eqn. 2). Electrostatic desolv: the loss of the DelPhi calculated solvation energy when the ligand is moved into the protein. Calc[2] with vdW[2] uses a -55 cal/mol/Å^2 SAS dependent implicit van der Waals energy for both ligand to protein and ligand to solvent interaction (Eqn. 4). TΔS: entropy correction due to expected loss of methoxy rotation degrees of freedom. All energy values are in kcal/mol.

A.	**1AIJ**	**Expt**	**Calc[1]**	**Calc[2]**	**SAS**	**TΔS**	**Electrostatics**							**vdW[1]**	**vdW[2]**
							De-solv	**bkbn**	**side chain**	**total**	**SAS**	**bkbn**	**side chain**	**total**	**total**
	unsub	**4.90**	**9.70**	**6.06**	-134	-0.80	-0.96	0.44	0.00	-0.52	0.67	6.11	3.12	9.90	7.37
	methyl	**4.60**	**6.62**	**4.04**	-107	-0.80	-0.62	0.11	-0.54	-1.06	0.54	6.58	-0.16	6.96	5.90
	2,3-dimethyl	**3.45**	**2.49**	**3.41**	-89	-0.80	-0.79	0.10	0.00	-0.70	0.45	4.86	-2.83	2.48	4.91
	2,5-dimethyl	**3.64**	**4.26**	**3.08**	-86	-0.80	-0.78	0.34	-0.41	-0.85	0.43	4.87	-0.50	4.80	4.73
	2,6-dimethyl	**3.63**	**3.96**	**3.42**	-79	-0.80	-1.04	0.88	0.00	-0.16	0.40	2.26	0.94	3.60	4.37
	tri-methyl	**1.52**	**2.04**	**1.87**	-61	-0.80	-0.94	0.37	-0.14	-0.70	0.31	3.22	-2.10	1.43	3.37
	tetra-methyl (DQ)	**-0.14**	**1.74**	**0.51**	-41	-0.80	-1.20	0.25	0.00	-0.95	0.21	5.97	-4.49	1.68	2.26
	2,6-dimethoxy	**2.73**	**-0.99**	**1.31**	-36	0.60	-0.10	0.20	-1.36	-1.26	0.18	1.11	-3.09	-1.80	1.98
	2,3-dimethoxy, 5-methyl (Q_0)	**1.59**	**2.60**	**0.71**	-14	0.00	0.05	0.17	-0.27	-0.06	0.07	2.18	0.18	2.43	0.77
	2,3-dimethoxy, 5,6-dimethyl (methyl-Q_0)*	**0.00**	**0.00**	**0.00**	0	0.00	0.00	0.00	0.00	0.00	0.00	0.00	0.00	0.00	0.00
	Absolute energies methyl Q_0						2.67	-1.49	-1.77	-0.59	-1.93	-14.01	-14.82	-30.76	

B.	2UWU	Expt	Calc[1]	Calc[2]	SAS Å^2	TΔS	Electrostatics							vdW[1]	vdW[2]
							De-solv	bkbn	side chain	total	SAS	bkbn	side chain	total	total
	Unsub	**4.90**	**7.15**	**6.83**	-134	-0.80	-1.17	0.61	0.82	0.26	0.67	4.71	1.21	6.59	7.37
	Methyl	**4.60**	**4.32**	**4.39**	-107	-0.80	-0.60	0.02	-0.13	-0.71	0.54	3.88	0.81	5.23	5.90
	2,3-dimethyl	**3.45**	**1.53**	**3.57**	-89	-0.80	-0.80	-0.01	0.27	-0.54	0.45	2.34	-1.11	1.68	4.91
	2,5-dimethyl	**3.64**	**1.86**	**3.25**	-86	-0.80	-0.74	0.20	-0.14	-0.68	0.43	1.72	0.28	2.43	4.73
	2,6-dimethyl	**3.63**	**3.28**	**3.35**	-79	-0.80	-1.12	0.49	0.41	-0.22	0.40	1.42	1.30	3.11	4.37
	tri-methyl	**1.52**	**1.89**	**1.28**	-61	-0.80	-0.91	-0.10	-0.27	-1.29	0.31	3.82	-0.77	3.35	3.37

A.	**1AIJ**	**Expt**	**Calc[1]**	**Calc[2]**	**SAS**	**TΔS**	**Electrostatics**							**vdW[1]**	**vdW[2]**
							De-solv	**bkbn**	**side chain**	**total**	**SAS**	**bkbn**	**side chain**	**total**	**total**
	tetra-methyl (DQ)	**-0.14**	**-0.21**	**0.83**	-41	-0.80	-1.16	0.26	0.27	-0.63	0.21	0.19	0.54	0.94	2.26
	2,6-dimethoxy	**2.73**	**-2.84**	**1.39**	-36	0.60	-0.05	0.09	-1.22	-1.18	0.18	-0.26	-3.17	-3.25	1.98
	2,3-dimethoxy, 5-methyl (Q_0)	**1.59**	**3.45**	**0.65**	-14	0.00	-0.06	0.48	-0.54	-0.12	0.07	-2.28	5.23	3.01	0.77
	2,3-dimethoxy, 5,6-dimethyl (methyl-Q_0)*	**0.00**	**0.00**	**0.00**	0	0.00	0.00	0.00	0.00	0.00	0.00	0.00	0.00	0.00	0.00
	Absolute energies methyl Q_0						2.68	-1.23	-1.77	-0.33	-1.93	-12.29	-15.22	-29.44	

C.	1AIJ	Expt	Calc[1]	Calc[2]	SAS	TΔS	Electrostatics							vdW[1]	vdW[2]
							De-solv	bkbn	side chain	total	SAS	bkbn	side chain	total	total
	Unsub	**-3.54**	**-21.76**	**-14.98**	252	0.00	1.71	-1.05	-1.77	-1.11	-1.26	-7.89	-11.70	-20.86	-13.88
	Methyl	**-3.84**	**-24.85**	**-17.00**	279	0.00	2.04	-1.38	-2.31	-1.65	-1.40	-7.42	-14.98	-23.80	-15.35
	2,3-dimethyl	**-4.98**	**-28.98**	**-17.63**	297	0.00	1.87	-1.39	-1.77	-1.29	-1.49	-9.14	-17.66	-28.29	-16.34
	2,5-dimethyl	**-4.79**	**-27.20**	**-17.96**	300	0.00	1.88	-1.14	-2.18	-1.44	-1.50	-9.14	-15.33	-25.97	-16.52
	2,6-dimethyl	**-4.80**	**-27.50**	**-17.62**	307	0.00	1.63	-0.61	-1.77	-0.75	-1.53	-11.74	-13.88	-27.16	-16.88
	tri-methyl	**-6.91**	**-29.43**	**-19.17**	325	0.00	1.73	-1.12	-1.90	-1.29	-1.63	-10.78	-16.93	-29.34	-17.88
	tetra-methyl (DQ)	**-8.57**	**-29.73**	**-20.53**	345	0.00	1.47	-1.24	-1.77	-1.54	-1.73	-8.04	-19.31	-29.08	-19.00
	2,6-dimethoxy	**-5.70**	**-32.45**	**-19.73**	350	1.40	2.57	-1.29	-3.13	-1.85	-1.75	-12.89	-17.92	-32.56	-19.27
	2,3-dimethoxy, 5-methyl (Q_0)	**-6.84**	**-28.86**	**-20.32**	372	0.80	2.72	-1.32	-2.04	-0.65	-1.86	-11.82	-14.64	-28.33	-20.48
	2,3-dimethoxy, 5,6-dimethyl (methyl-Q_0)*	**-8.43**	**-31.46**	**-21.04**	386	0.80	2.67	-1.49	-1.77	-0.59	-1.93	-14.01	-14.82	-30.76	-21.25

*methyl Q_0 is chosen as the reference compound. The Calc[1] energies are derived from the quinone solution chemical potential needed to have equal amounts of quinone bound and free in Monte Carlo sampling. The energy breakdown is obtained using equation 1. This uses a mean field analysis given the conformer distribution generated by the Monte Carlo sampling under conditions where half of the proteins have quinone bound.

Table 2

Expt: measured values; $Calc^{single}$: Single GROMACS minimized backbone, side chain and quinone position is evaluated with a QUICK calculation where only side chain isosteric and protonation conformers are sampled (see table S1); $Calc^{1}$ and $Calc^{2}$ are defined as in Table 1. $Calc^{scale}$: a scaling factor of 0.62 is applied to all protein-ligand van der Waals interactions. Range is the difference in affinity between the tightest and weakest binding quinone in kcal/mol. The other terms characterize the correspondence between the calculated and experimental relative affinities.

	Expt	$Calc^{single}$	$Calc^{1}$	$Calc^{scale}$	$Calc^{2}$
range	5.04	10.7	10.7	6.7	5.5
slope	n/a	0.016	1.28	0.81	0.97
R^2	n/a	0	0.54	0.78	0.84
avg. abs. error	n/a	3.46	1.76	1.14	0.64
RMSD	n/a	4.2	2.29	1.4	0.77